LANGMUIR

pubs.acs.org/Langmuir Article

Possibility of Obtaining Two Orders of Magnitude Larger Electrokinetic Streaming Potentials, through Liquid Infiltrated Surfaces

Bei Fan and Prabhakar R. Bandaru*

Cite This: *Langmuir* 2020, 36, 10238−10243

Read Online

ACCESS | Metrics & More | Article Recommendations

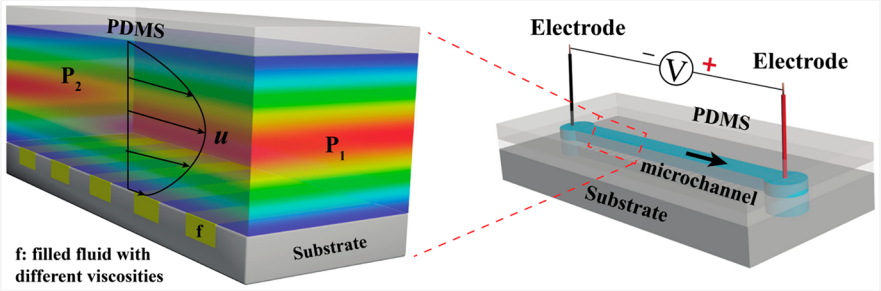

ABSTRACT: It is shown that the magnitude of the streaming potential (V_s) can be significantly enhanced from ∼0.02 V to as much as ∼1.6 V, in electrokinetic flows through microchannels. This was done through flows on liquid-filled surfaces, where the grooves were filled with oils of viscosity in the range 30−3000 mPa·s. The presence of immiscible oils and the improved slip are both factors that could significantly increase the V_s. The analytical relationship between streaming potential and filled liquid viscosity was derived and verified through corresponding experimental results. The work yields novel insights into complex electrolyte flows and indicates avenues for more efficient energy harvesting.

INTRODUCTION

The motion of electrolyte fluid relative to a surface[1,2] is of significant relevance for insight into the effects of charge accumulation as well as dispersion and may be widely applicable to electrical power generation[3−5] as well as biological processes.[6,7] The significant electrokinetic effects, driven by the pressure gradient along the microchannel, incorporate (1) an electrical streaming current (I_s), due to ion movement inside an electrical double layer (EDL) proximate to the channel surface, and (2) a voltage (the electrokinetic streaming potential V_s) under open electrical circuit conditions, due to charge separation between the ends of the channel. The V_s may be further increased through deploying nanometer scale fluidic channels,[3,8,9] e.g., through the convergence of EDLs from the top and bottom surfaces, enabling flow of ions of a particular polarity, as in batteries.

Fluid flow over hydrodynamically smooth surfaces with assumed no-slip conditions nominally yields low I_s and V_s. It was suggested that improved mobility, M, may be harnessed using patterned[10,11] or superhydrophobic (SH) surfaces,[12] in a large range of Reynold number (Re) flows. Pertinent to SH surfaces[12] is the ion mobility,[13] $M = \frac{\varepsilon\zeta}{\eta_e}$, where ε ($=\varepsilon_0\varepsilon_r$; $\varepsilon_0 = 8.854 \times 10^{-12}$ C^2/N m^2 is the permittivity of vacuum and ε_r is the dielectric constant) is the overall permittivity of the electrolyte, ζ is the magnitude of the zeta potential, and η_e is the electrolyte viscosity. It requires[14−16] that the surfaces promoting the liquid slip have a finite charge density, of related value to that of a no-slip surface. Traditionally, SH surfaces have been constituted through roughness on the fluid slipping surface[17−19] or through lithographic patterning,[20,21] which in either case exploits air in the surface to promote slip. In the context of electrokinetic flows, air would not be useful as it was conclusively stated that only a charged liquid−air interface would, in principle, increase the V_s.[14−16] There is indeed considerable ambiguity as to whether charge exists on the air−electrolyte interface, e.g., due to residual OH^- ions.[16] Consequently, when the slipping surface is even partially devoid of charges, the V_s could be lower compared to the streaming potential that could be obtained from a homogeneously charged smooth surface,[14,15] and such assertions were indeed validated previously.[22]

Received: June 16, 2020
Revised: August 4, 2020
Published: August 6, 2020

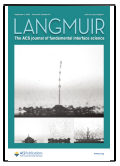

https://dx.doi.org/10.1021/acs.langmuir.0c01771
Langmuir 2020, 36, 10238−10243

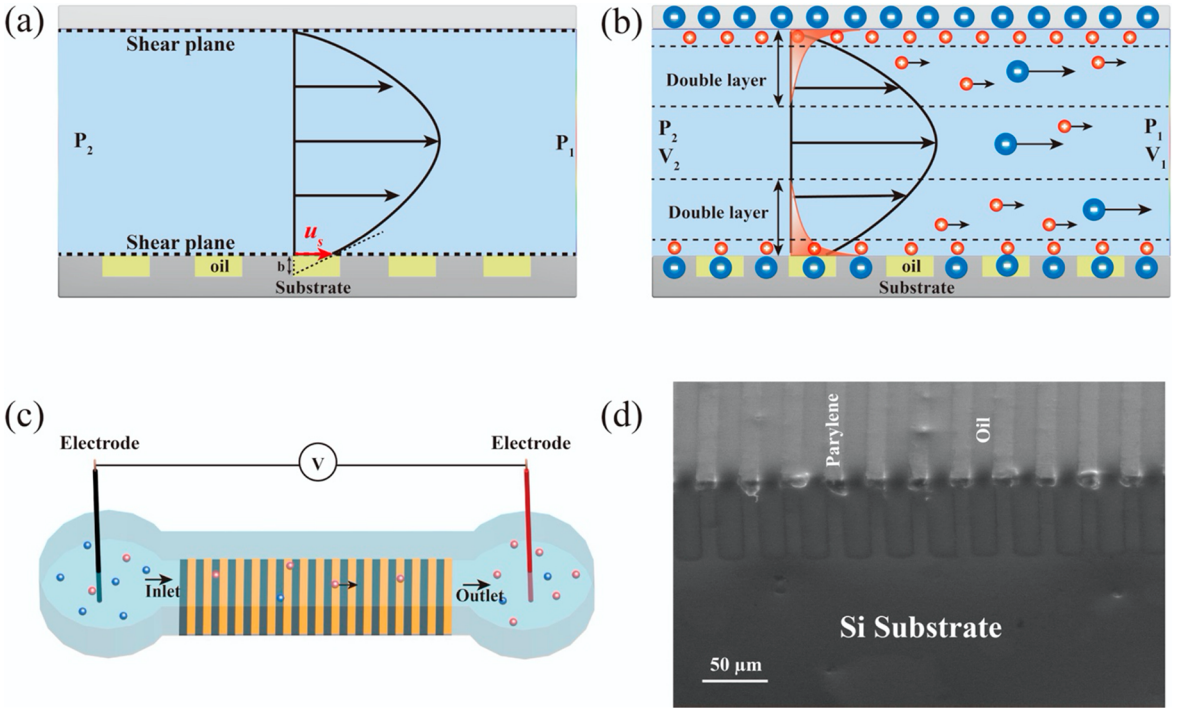

Figure 1. Electrokinetic flows under Poiseuille flow (with a difference of the pressures between the entrance and exit of the channel, $\Delta P = P_1 - P_2$) on the liquid-filled surfaces (LFS). The (a) finite slip velocity (u_s) at the interface, along with (b) a charged electrolyte−oil interface, ensures an enhanced streaming potential ($V_s = V_1 - V_2$). (c) Experimental measurement of the V_s (related to the measured voltage difference V, across the electrodes at the end) ensuing from pressure driven flow of salt water. (d) Image, based on scanning electron microscopy (SEM), of LFS filled by GPL oil.

As an alternative to conventional surfaces, where the grooves are comprised of air, liquid-filled surfaces (LFS), fabricated by oil filled into interstices of rectangular grooves on the surface, were studied in this work. The advantages of an LFS, constituted from liquid as well as the intervening hydrophobic solid surface, are that a finite charge density would be ensured at the slipping surface in addition to a finite slip velocity.[23] The frictional drag[24−26] between the flowing electrolyte and a solid surface could also be diminished. Figure 1a is a schematic of the flow (indicating the slip velocity u_s and related slip length b), while Figure 1b shows the electrokinetic flow patterns, over the LFS. Moreover, previous work[22] introducing the LFS for enhancing V_s has shown that a larger than 2-fold increase in the V_s may be obtained through the use of specific oils in the LFS. While finite charge at the electrolyte−oil interface may provide a possible reason for the increase, the rationale for the choice of the filling liquid, say, with respect to the fluid slip has been unclear. Additionally, filled oil properties[27] and groove orientation[28] may also be influential. Here, we discuss specific correlations between the viscosity of the filling liquid in the LFS with the V_s through analysis and experimental results. We aim to provide a deeper understanding and new perspectives on electrokinetic flows through such investigations.

EXPERIMENTAL SECTION

Fabrication and Characterization of LFS. The LFS was fabricated by infiltrating a series of oils with systematically varying viscosities into lithographically groove patterned channels. The bare channel fabrication and related details have been reported.[27] Here, we show the V_s modulations obtained through related filling liquid variations, from an LFS with a fixed groove width (w = 18 μm) and period L ($=w + d$) = 36 μm. We define a groove fraction, $\phi = w/L$, to characterize the patterned surfaces. The η_{oil} was varied over 2 orders of magnitude (in the range 30−3000 mPa·s), as indicated in Table 1, for probing the electrokinetic potentials. The oils (Dupont Krytox GPL), were found to be not miscible with the NaCl electrolyte. GPL (general purpose lubricant) represents a family of widely used perfluorinated oils known to be inert and stable over a wide temperature range. The oil spillage out of the grooves in the pattern was considered negligible due to the enhanced surface tension forces, and was also verified through microscopy.[27]

Table 1. Viscosity of the Oils Deployed in the LFS

oil	η_{oil} (mPa·s)
GPL 101	33
GPL 102	73
GPL 104	341
GPL 105	1012
GPL 107	2993

Streaming Potential V_s Measurement. The V_s was monitored in a microfluidics-based setup, with a microchannel (~250 μm in height, a length of 11.8 cm, and a width of 0.9 cm) using salt water (with NaCl dissolved in water at a concentration of 0.1 mM) under pressure driven Poiseuille flow (Figure 1c and Figure 2). The upper surface of the channel was silicone coated onto polycarbonate, while the lower surface was the LFS. The two surfaces in the microchannel were placed at a fixed height using a silicone rubber spacer, and electrodes (Ag/AgCl) at either end were deployed to measure the potential difference for the V_s. The pressure drop (ΔP) along the channel length was varied in the 200−1200 Pa range, monitored (UEI EM152 manometer), and checked to be in correspondence with the Poiseuille flow. The chosen pressure range yielded reliable and reproducible V_s values. Experiments were performed with the flow direction perpendicular to the grooves considering the stability of the LFS, i.e., whether the filling oil would experience shear-induced drainage under external flow.[29] The liquid filling the LFS could be

https://dx.doi.org/10.1021/acs.langmuir.0c01771
Langmuir 2020, 36, 10238−10243

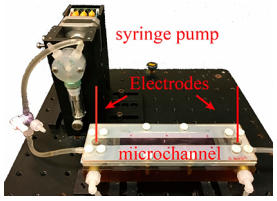

Figure 2. Experimental realization for measuring the streaming potential V_s. The top surface of the microchannel was separated by a silicone rubber spacer from the bottom surface to yield a fixed height. Electrodes were placed in the reservoirs at two ends of the channel to measure the potential differences/voltage.

contained indefinitely inside the grooves in such a configuration,[28] if the groove period was smaller compared to the critical length scale[29] L_∞, inversely proportional to the w/h ratio. For the given experimental conditions, L_∞ was at the millimeter scale, and it was assumed from such consideration as well from SEM observations after the experiments (Figure 1d) that the LFS are stable. The V_s was monitored six times for each particular pressure, for estimating the mean and the deviation.

RESULTS AND DISCUSSION

Influence of the Slip Length in Modulating Streaming Potentials. Electrokinetic flow of an electrolyte, under a pressure difference (ΔP), has been conventionally modeled through the Helmholtz−Smoluchowski (H−S) relation, which is of the form[30,31] $V_s = \frac{M}{\sigma}\Delta P$, with σ as the electrolyte conductivity. The relation is valid for homogeneous and smooth surfaces. Further assumptions[32] underlying the relation include neglecting surface (substrate) conduction and very thin EDL thickness.[33] Also incorporated is the no-slip boundary condition,[34] with a nonzero flow up to a definitive distance (the shear plane boundary), away from the substrate surface, into the liquid electrolyte. ζ is considered to the electrical potential at the shear plane.[31,32] To date, V_s has mostly been considered through flows over nonrough surfaces (where the mean roughness scale is smaller compared to the Debye length λ_D), and consequently the use of the H−S relation implies millivolt levels of the measured V_s;[30] e.g., with $\Delta P \sim 1000$ Pa, and 0.1 mM NaCl, $\varepsilon_r \sim 80$, $\eta_e \sim 10^{-3}$ Pa·s, $\zeta \sim 25$ mV, $\sigma \sim 10^{-3}$ S/m, and $V_s \sim 18$ mV.

Molecular dynamics (MD) modeling and simulations[35] have indicated that slip could be responsible for the mobilization of the Stern layer and, consequently, enhance ζ. Due to the slip, the shear plane would be moved closer to the surface. As the magnitude of the electrical potential is exponentially diminished away from the surface, a proximate shear plane may yield a larger ζ with increased V_s, per the H−S relation. Alternate to the no-slip boundary condition at the surface ($y = 0$) would be a condition (corresponding to Navier slip):

$$u_s(y=0) = b\,\frac{\partial u(y=0)}{\partial y}$$

with b the slip length,[36,37] and u_s the slip velocity (Figure 1a). The V_s will be enhanced over that predicted through the H−S relation, by a factor $\frac{b_{eff}}{\lambda_D}$, where b_{eff} is the effective slip length—an average local slip length[30]—i.e.

$$V_s = \frac{\varepsilon\zeta}{\eta_e\sigma}\Delta P\left(1 + \frac{b_{eff}}{\lambda_D}\right) \tag{1}$$

For a rectangular groove patterned surface, b_{eff} in directions parallel (i.e., $b_{eff}^{\parallel}$), and that perpendicular ($b_{eff}^{\perp}$) to the grooves[38,39] may be estimated through the following relations:

$$b_{eff}^{\parallel} = \frac{L}{\pi}\frac{\ln\left[\sec\left(\frac{\pi\phi}{2}\right)\right]}{1 + \frac{L}{\pi b}\ln\left[\sec\left(\frac{\pi\phi}{2}\right) + \tan\left(\frac{\pi\phi}{2}\right)\right]} \tag{2}$$

$$b_{eff}^{\perp} = \frac{L}{2\pi}\frac{\ln\left[\sec\left(\frac{\pi\phi}{2}\right)\right]}{1 + \frac{L}{2\pi b}\ln\left[\sec\left(\frac{\pi\phi}{2}\right) + \tan\left(\frac{\pi\phi}{2}\right)\right]} \tag{3}$$

L ($=w + d$) is the groove pattern period with w as the groove width and d constituting the longitudinal length of the solid part of the LFS; $b = w\frac{\eta_e}{\eta_{oil}}\beta$ is the local constant slip length and η_{oil} is the viscosity of the liquid (oil) in the grooves.[38] Generally, β has been modeled with different values for parallel and transverse grooves,[38] i.e.

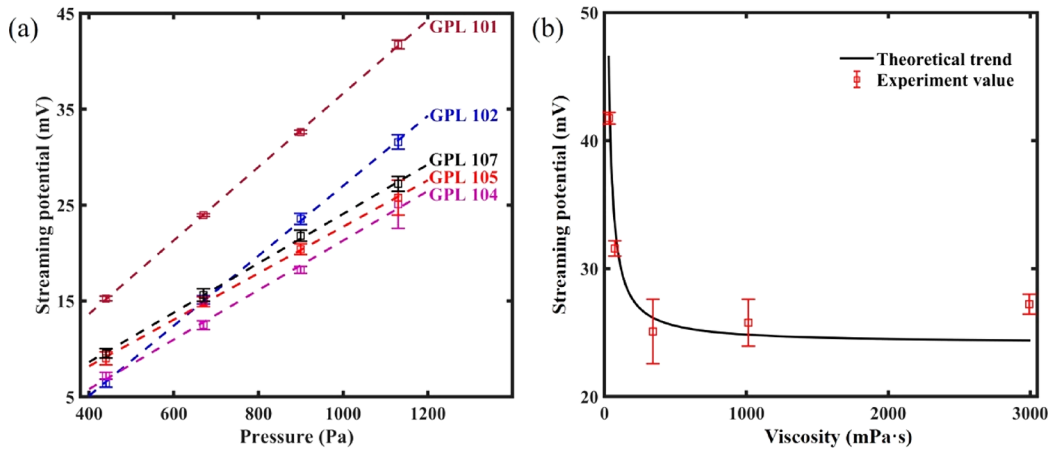

Figure 3. (a) Measured streaming potential (V_s) on liquid filled surface (LFS) using a series of GPL oils, of varying viscosity, with 0.1 mM NaCl as the electrolyte solution scales linearly with the applied pressure drop. (b) Comparison of experimentally measured V_s (when the pressure drop ΔP = 1130 Pa) to the analytical relationship of eq 4.

https://dx.doi.org/10.1021/acs.langmuir.0c01771
Langmuir 2020, 36, 10238−10243

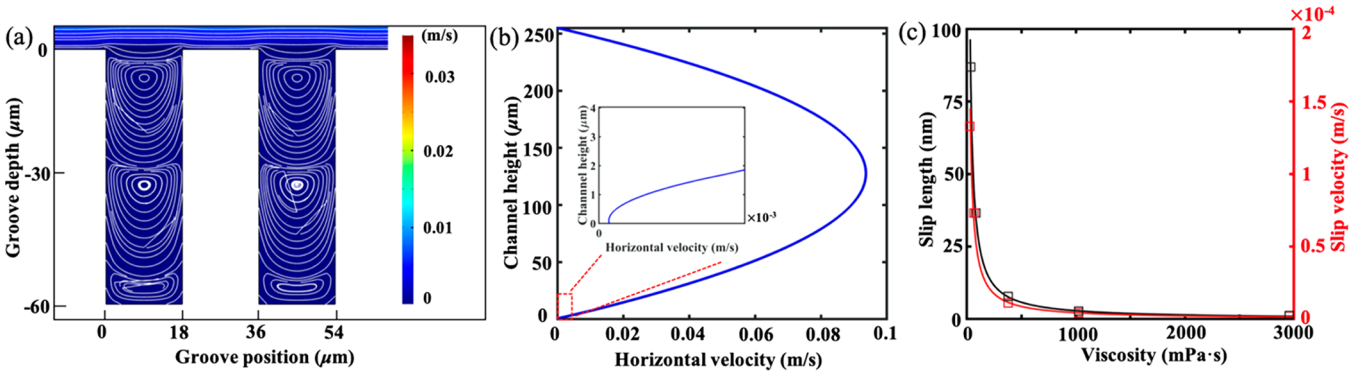

Figure 4. (a) Simulated flow velocity near the grooves for oil (GPL 101) filled liquid filled surfaces (LFS) with groove height h = 60 μm, groove width w = 18 μm. (b) Velocity profile between the liquid−oil interface (bottom) and the upper surface of the microchannel; the inset indicates nonzero slip, i.e., a finite u_s, at the liquid−oil interface. (c) Simulated slip length (left axis) and slip velocity (right axis) scale inversely as the oil viscosity (at ΔP = 1130 Pa).

$$\beta_{\parallel} = \frac{\mathrm{erf}\left(\frac{q_x h}{w}\right)}{q_x} \quad \text{and} \quad \beta_{\perp} = \frac{\mathrm{erf}\left(\frac{q_y h}{w}\right)}{4q_y}$$

where h is the groove depth, $q_x \simeq 3.1$, and $q_y \simeq 2.17$. When $h/w \gg 1$, as in our case, with $h \sim 100$ μm and $w \sim 18$ μm, $\beta_{\parallel}$ and $\beta_{\perp}$ may be estimated to be ∼0.32 and ∼0.12, respectively. Consolidating the above relationships, it was derived that

$$V_s = \frac{\varepsilon\zeta}{\eta_e \sigma}\Delta P\left(1 + \frac{m}{1 + n\eta_{oil}}\right) \tag{4}$$

Here, m and n are two groove geometry-dependent parameters, i.e., for parallel grooves

$$m_{\parallel} = \frac{L}{\pi}\frac{\ln\left[\sec\left(\frac{\pi\phi}{2}\right)\right]}{\lambda_D}, \quad n_{\parallel} = \frac{L}{\pi}\frac{\ln\left[\sec\left(\frac{\pi\phi}{2}\right) + \tan\left(\frac{\pi\phi}{2}\right)\right]}{w\beta\eta_e} \tag{5}$$

while for transverse grooves

$$m_{\perp} = \frac{L}{2\pi}\frac{\ln\left[\sec\left(\frac{\pi\phi}{2}\right)\right]}{\lambda_D}, \quad n_{\perp} = \frac{L}{2\pi}\frac{\ln\left[\sec\left(\frac{\pi\phi}{2}\right) + \tan\left(\frac{\pi\phi}{2}\right)\right]}{w\beta\eta_e} \tag{6}$$

The aim was to experimentally verify eq 4 with an explicit consideration of the nature of the LFS, to yield insights into the influence of surfaces on electrokinetic behavior.

Pressure Induced Modulation of the V_s on LFS Constituted from Oils of Different Viscosities. The measured V_s values as a function of ΔP are in general accord with the H−S relation, through the obtained linear variations for different LFS (Figure 3a). For 0.1 mM NaCl solution, with a Debye length $\lambda_D \sim 30$ nm, we estimate, from eq 6, $m_{\perp}$ = 66.2 and $n_{\perp}$ = 2.3. The ζ of LFS was estimated to be ∼30.9 mV. Inserting the numerically obtained values into eq 4 with ΔP = 1130 Pa, we obtain the following relation between V_s and η_{oil} for the LFS:

$$V_s\ (\mathrm{mV}) = 24.15\left(1 + \frac{66.19}{1 + 2.34\eta_{oil}\ (\mathrm{mPa{\cdot}s})}\right) \tag{7}$$

A comparison of the experimentally obtained V_s with the analytically evaluated eq 7 is indicated in Figure 3b and shows excellent agreement (R^2 = 0.99). Based on such an agreement, we predict an even larger V_s with smaller η_{oil}. Indeed, use of aqueous media (with $\eta \sim 1$ mPa·s) or hydrocarbon-based liquids (with $\eta \sim 0.2$ mPa·s) would yield V_s values of the order of 0.5 and 1.1 V, respectively. The relationship also allows us to predict an upper limit to the V_s, obtained when η tends to zero, of ∼1.6 V, approaching the voltages that could be obtained from conventional batteries.

Modeling Fluid Flow over the LFS. We used finite element methodologies (FEM), deploying the incompressible Navier−Stokes equations, to model the fluid flow over LFS with η_{oil} in the groove over the range of values in Table 1 based on a two-phase flow (laminar) level set model, over a given groove. The level set method (with a concomitant function ϕ) was used to trace the electrolyte−oil interface, interpolating between the electrolyte (with ϕ = 0) and the oil (with ϕ = 1). The interface was located at where ϕ = 0.5. At the interface, the local density ρ_l and dynamic viscosity η_l are determined based on the smooth step level set function and are equal to

$$\rho_l = \rho_w + (\rho_o - \rho_w)\phi \tag{8}$$

$$\eta_l = \eta_w + (\eta_o - \eta_w)\phi \tag{9}$$

ρ_w is the water density and η_w is the dynamic viscosity of water, while ρ_o and η_o are the corresponding parameters for the oil. We used a creeping flow model which neglects inertial terms and sets the gravity body force to zero. A no-slip condition was used at the ridge surface−electrolyte boundary, and a Navier slip boundary condition was used at the oil−electrolyte boundary. The mass and momentum transport here were considered through the Navier−Stokes equations. Here, the surface tension dominates over the viscous forces, as may also be deduced from an estimate of $\sim 10^{-3}$ for the capillary number (Ca). Consequently, the flows are not expected to significantly perturb the flatness of the electrolyte−oil interface.[40] In our simulations, we used (1) rounding the sharp corner as well as (2) adaptive mesh methods to refine the mesh grids.

https://dx.doi.org/10.1021/acs.langmuir.0c01771
Langmuir 2020, 36, 10238−10243

When electrolyte flows above the LFS, the shear stress at the electrolyte−oil interface was implicated in the generation of vortices as shown in Figure 4a. The electrolyte flow in the channel was considered with nonzero slip velocity (u_s),[41] as in Figure 4b. The u_s and the slip length were inversely proportional to η_{oil} as indicated in Figure 4c.

The related shear rate was estimated from the velocity profile, and a corresponding fluid slip length (b_{sim}) was obtained from the Navier slip boundary condition. The b_{sim} was compared to the theoretical estimate, i.e., with b_{theo} $(=w\frac{\eta_e}{\eta_{oil}}\beta)$, in Table 2, and close correspondence was seen.

Table 2. Electrolyte Fluid Slip Length (b) from Simulations: b_{sim} in Comparison with Theoretical Estimates (b_{theo})

oil	b_{sim} (nm)	b_{theo} (nm)
GPL 101	87.0	65.0
GPL 102	40.9	30.0
GPL 104	8.7	6.3
GPL 105	3.0	2.1
GPL 107	1.0	0.7

CONCLUSIONS

The proposed work has indicated that streaming potentials, as large as 1.6 V, may possibly be obtained through the use of specifically structured surfaces, such as the LFS, in comparison to the typical values of ∼0.02 V using smooth surfaces or even conventional superhydrophobic surfaces. It was shown that the viscosity of the infiltrating oil in the LFS is critical to the obtained V_s. An analytically derived relationship was confirmed experimentally and has been used to predict the limits of the V_s. The LFS, in addition to enhancing the fluid slip velocity and slip length, provides a charged electrolyte−oil interface which may contribute to the plausible orders of magnitude enhancement of the V_s. While it was previously indicated that[9,42] that overlap of the EDLs in nanoscale channels may be necessary for boosting the magnitude of the electrokinetic potential, ensuring smooth flow and maintaining steady flow rate are constraints for practical implementation.[43] The presented work provides an alternative for achieving large V_s at the *micro*scale. With such plausibility, our results provide much motivation for aiming at more detailed understanding of electrokinetics on hybrid/nonhomogeneous surfaces and open new perspectives for guiding multiphase flow and related biology and energy-harvesting applications.

AUTHOR INFORMATION

Corresponding Author

Prabhakar R. Bandaru − *Program in Materials Science, Department of Mechanical & Aerospace Engineering, University of California—San Diego, La Jolla, California 92093, United States;* orcid.org/0000-0003-4497-9620; Phone: (858) 534-5325; Email: pbandaru@ucsd.edu

Author

Bei Fan − *Program in Materials Science, Department of Mechanical & Aerospace Engineering, University of California—San Diego, La Jolla, California 92093, United States*

Complete contact information is available at: https://pubs.acs.org/10.1021/acs.langmuir.0c01771

Notes

The authors declare no competing financial interest.

ACKNOWLEDGMENTS

The authors are thankful for support from the National Science Foundation (NSF; CBET 1606192). We also acknowledge discussions with Prof. J. Friend and Dr. S. Rubin.

REFERENCES

(1) Morrison, F. A., Jr.; Osterle, J. F. Electrokinetic Energy Conversion in Ultrafine Capillaries. *J. Chem. Phys.* **1965**, *43*, 2111.

(2) Quincke, G. Ueber Eine Neue Art Elektrischer Ströme. *Ann. Phys.* **1859**, *183* (5), 1−47.

(3) Yang, J.; Lu, F.; Kostiuk, L. W.; Kwok, D. Y. Electrokinetic Microchannel Battery by Means of Electrokinetic and Microfluidic Phenomena. *J. Micromech. Microeng.* **2003**, *13* (6), 963−970.

(4) Olthuis, W.; Schippers, B.; Eijkel, J.; Van Den Berg, A. Energy from Streaming Current and Potential. *Sens. Actuators, B* **2005**, *111*−*112*, 385−389.

(5) Pennathur, S.; Eijkel, J. C. T.; van den Berg, A. Energy Conversion in Microsystems: Is There a Role for Micro/Nanofluidics? *Lab Chip* **2007**, *7*, 1234−1237.

(6) Madou, M. *Fundamentals of Microfabrication*, 2nd ed.; CRC Press: Boca Raton, FL, 2002.

(7) Hunter, R. J. *Foundations of Colloid Science*; Oxford University Press: Oxford, U.K., 2001.

(8) Daiguji, H.; Yang, P.; Szeri, A. J.; Majumdar, A. Electrochemomechanical Energy Conversion in Nanofluidic Channels. *Nano Lett.* **2004**, *4*, 2315.

(9) van der Heyden, F. H. J.; Bonthuis, D. J.; Stein, D.; Meyer, C.; Dekker, C. Electrokinetic Energy Conversion Efficiency in Nanofluidic Channels. *Nano Lett.* **2006**, *6* (10), 2232−2237.

(10) Battiato, I. Effective Medium Theory for Drag-Reducing Micro-Patterned Surfaces in Turbulent Flows. *Eur. Phys. J. E: Soft Matter Biol. Phys.* **2014**, *37*, 19.

(11) Battiato, I.; Bandaru, P. R.; Tartakovsky, D. M. Elastic Response of Carbon Nanotube Forests to Aerodynamic Stresses. *Phys. Rev. Lett.* **2010**, *105*, 144504.

(12) Papadopoulos, P.; Deng, X.; Vollmer, D.; Butt, H.-J. Electrokinetics on Superhydrophobic Surfaces. *J. Phys.: Condens. Matter* **2012**, *24* (46), 464110.

(13) Dukhin, S. S. Development of Notions as to the Mechanism of Electrokinetic Phenomena and the Structure of the Colloid Micelle. In *Surface and Colloid Science*; John Wiley & Sons: New York, NY, 1974; pp 1−47.

(14) Squires, T. M. Electrokinetic Flows over Inhomogeneously Slipping Surfaces. *Phys. Fluids* **2008**, *20* (9), 092105.

(15) Bahga, S. S.; Vinogradova, O. I.; Bazant, M. Z. Anisotropic Electro-Osmotic Flow over Super-Hydrophobic Surfaces. *J. Fluid Mech.* **2010**, *644*, 245−255.

(16) Zhao, H. Electro-Osmotic Flow over a Charged Superhydrophobic Surface. *Phys. Rev. E - Stat. Nonlinear, Soft Matter Phys.* **2010**, *81* (6), 066314.

(17) Moreira, D.; Park, S.; Lee, S.; Verma, N.; Bandaru, P. R. Dynamic Superhydrophobic Behavior in Scalable Random Textured Polymeric Surfaces. *J. Appl. Phys.* **2016**, *119* (12), 125302.

(18) Park, S.-H.; Lee, S.; Moreira, D.; Bandaru, P. R.; Han, I.; Yun, D.-J. Bioinspired Superhydrophobic Surfaces, Fabricated through Simple and Scalable Roll-to-Roll Processing. *Sci. Rep.* **2015**, *5*, 15430.

(19) Moreira, D.; Bandaru, P. R. Thermal Transport in Laminar Flow over Superhydrophobic Surfaces, Utilizing an Effective Medium Approach. *Phys. Fluids* **2015**, *27* (5), 052001.

(20) Ybert, C.; Barentin, C.; Cottin-Bizonne, C.; Joseph, P.; Bocquet, L. Achieving Large Slip with Superhydrophobic Surfaces: Scaling Laws for Generic Geometries. *Phys. Fluids* **2007**, *19* (12), 123601.

https://dx.doi.org/10.1021/acs.langmuir.0c01771
Langmuir 2020, 36, 10238−10243

(21) Joly, L.; Ybert, C.; Trizac, E.; Bocquet, L. Hydrodynamics within the Electric Double Layer on Slipping Surfaces. *Phys. Rev. Lett.* **2004**, *93*, 257805.
(22) Fan, B.; Bhattacharya, A.; Bandaru, P. R. Enhanced Voltage Generation through Electrolyte Flow on Liquid-Filled Surfaces. *Nat. Commun.* **2018**, *9*, 4050.
(23) Ren, Y.; Stein, D. Slip Enhanced Electrokinetic Energy Conversion in Nanofluidic Channels. *Nanotechnology* **2008**, *19*, 195707.
(24) Sadullah, M. S.; Semprebon, C.; Kusumaatmaja, H. Drop Dynamics on Liquid Infused Surfaces: The Role of the Wetting Ridge. *Langmuir* **2018**, *34*, 8112.
(25) Solomon, B. R.; Khalil, K. S.; Varanasi, K. K. Drag Reduction Using Lubricant-Impregnated Surfaces in Viscous Laminar Flow. *Langmuir* **2014**, *30* (36), 10970−10976.
(26) Schönecker, C.; Hardt, S. Assessment of Drag Reduction at Slippery, Topographically Structured Surfaces. *Microfluid. Nanofluid.* **2015**, *19* (1), 199−207.
(27) Fan, B.; Bandaru, P. R. Modulation of the Streaming Potential and Slip Characteristics in Electrolyte Flow over Liquid-Filled Surfaces. *Langmuir* **2019**, *35* (18), 6203−6210.
(28) Fan, B.; Bandaru, P. R. Tensorial Modulation of Electrokinetic Streaming Potentials on Air and Liquid Filled Surfaces. *Langmuir* **2019**, *35* (46), 14812−14817.
(29) Wexler, J. S.; Jacobi, I.; Stone, H. A. Shear-Driven Failure of Liquid-Infused Surfaces. *Phys. Rev. Lett.* **2015**, *114* (16), 168301.
(30) Kirby, B. J. *Micro- and Nanoscale Fluid Mechanics: Transport in Microfluidic Devices*; Cambridge University Press: 2010.
(31) Kirby, B. J.; Hasselbrink, E. F. Zeta Potential of Microfluidic Substrates: 1. Theory, Experimental Techniques, and Effects on Separations. *Electrophoresis* **2004**, *25*, 187−202.
(32) Hunter, R. J. *Zeta Potential in Colloid Science: Principles and Applications*; Academic Press: San Diego, CA, 1986.
(33) Israelachvili, J. N. *Intermolecular and Surface Forces*, 3rd ed.; Academic Press: San Diego, CA, 2011.
(34) Kundu, P. K.; Cohen, I. M. *Fluid Mechanics*, 4th ed.; Academic Press: San Diego, CA, 2008.
(35) Joly, L.; Ybert, C.; Trizac, E.; Bocquet, L. L. Hydrodynamics within the Electric Double Layer on Slipping Surfaces. *Phys. Rev. Lett.* **2004**, *93* (25), 257805.
(36) Bocquet, L.; Lauga, E. A Smooth Future? *Nat. Mater.* **2011**, *10* (5), 334−337.
(37) Joseph, P.; Cottin-Bizonne, C.; Benoit, J.-M.; Ybert, C.; Journet, C.; Tabeling, P.; Bocquet, L. Slippage of Water Past Superhydrophobic Carbon Nanotube Forests in Microchannels. *Phys. Rev. Lett.* **2006**, *97*, 156104.
(38) Nizkaya, T. V.; Asmolov, E. S.; Vinogradova, O. I. Gas Cushion Model and Hydrodynamic Boundary Conditions for Superhydrophobic Textures. *Phys. Rev. E - Stat. Nonlinear, Soft Matter Phys.* **2014**, *90* (4), 043017.
(39) Belyaev, A. V.; Vinogradova, O. I. Effective Slip in Pressure-Driven Flow Past Super-Hydrophobic Stripes. *J. Fluid Mech.* **2010**, *652*, 489.
(40) Asmolov, E. S.; Nizkaya, T. V.; Vinogradova, O. I. Enhanced Slip Properties of Lubricant-Infused Grooves. *Phys. Rev. E: Stat. Phys., Plasmas, Fluids, Relat. Interdiscip. Top.* **2018**, *98*, 033103.
(41) Maduar, S. R.; Belyaev, A. V.; Lobaskin, V.; Vinogradova, O. I. Electrohydrodynamics near Hydrophobic Surfaces. *Phys. Rev. Lett.* **2015**, *114*, 118301.
(42) van der Heyden, F. H. J.; Bonthuis, D. J.; Stein, D.; Meyer, C.; Dekker, C. Power Generation by Pressure-Driven Transport of Ions in Nanofluidic Channels. *Nano Lett.* **2007**, *7*, 1022−1025.
(43) Zhang, X.; Tartakovsky, D. M. Effective Ion Diffusion in Charged Nanoporous Materials. *J. Electrochem. Soc.* **2017**, *164*, E53−E61.

https://dx.doi.org/10.1021/acs.langmuir.0c01771
Langmuir 2020, 36, 10238−10243